HHS Public Access

Author manuscript

Ultrasound Med Biol. Author manuscript; available in PMC 2017 April 01.

Published in final edited form as:

Ultrasound Med Biol. 2016 April ; 42(4): 909–918. doi:10.1016/j.ultrasmedbio.2015.11.025.

Classification of Symptomatic and Asymptomatic Patients with and without Cognitive Decline using Non-invasive Carotid Plaque Strain Indices as Biomarkers

X. Wang[1], **D.C. Jackson**[2], **C.C. Mitchell**[3], **T. Varghese**[1], **S.M. Wilbrand**[4], **B.G. Rocque**[4], **B.P. Hermann**[2], and **R. J. Dempsey**[4]

[1]Department of Medical Physics, University of Wisconsin School of Medicine and Public Health, University of Wisconsin-Madison, Madison, WI-53706

[2]Department of Neurology, University of Wisconsin School of Medicine and Public Health, University of Wisconsin-Madison, Madison, WI-53706

[3]Department of Medicine, University of Wisconsin School of Medicine and Public Health, University of Wisconsin-Madison, Madison, WI-53706

[4]Department of Neurological Surgery, University of Wisconsin School of Medicine and Public Health, University of Wisconsin-Madison, Madison, WI-53706

Abstract

Vascular cognitive decline may be caused by micro-emboli generated from carotid plaque instability. We have previously shown that maximum strain indices in carotid plaque were significantly correlated with cognitive function. In this paper, we examine these associations with a larger sample size, along with performance evaluation of these maximum strain indices to predict cognitive impairment. Ultrasound-based strain imaging and cognition assessment were conducted on 75 human subjects. Patients underwent one of two standardized cognitive test batteries, using either the Repeatable Battery for the Assessment of Neuropsychological Status (RBANS) or the National Institute of Neurological Disorder and Stroke-Canadian Stroke Network (NINDS-CSN) Vascular Cognitive Impairment Harmonization Standards (60-minute). Scores were standardized within each battery to allow these data to be combined across all participants. Radiofrequency signals for ultrasound strain imaging were acquired on the carotid arteries using either a Siemens Antares with a VFX 13-5 linear array transducer or a Siemens S2000 with a 18L6 linear array transducer. The same hierarchical block-matching motion tracking algorithm developed in our laboratory was utilized to estimate accumulated axial, lateral, and shear strain indices in carotid plaque with inclusion of adventitia regardless of the ultrasound system and transducer used. Associations between cognitive z-scores and maximum strain indices were examined using Pearson's correlation coefficients. Maximum strain indices were also utilized to

Address all correspondence to: Xiao Wang, Ph.D., Department of Medical Physics, University of Wisconsin School of Medicine and Public Health, University of Wisconsin-Madison, Madison, WI 53706, USA. **Voice:** (608)-265-8797, **Fax:** (608)-262-2413, xwang235@wisc.edu, tvarghese@wisc.edu.

predict cognitive impairment using ROC analysis. All correlations between maximum strain indices and total cognition were statistically significant ($p<0.05$), indicating that these indices have good utility for predicting cognitive impairment. Maximum lateral strain indices provide an AUC of 0.85 for symptomatic patients, and 0.68 for asymptomatic patients. Our results demonstrate the important relationship of maximum strain indices and cognitive function, and the feasibility of using maximum strain indices to predict cognitive decline with inclusion of adventitia layer into the segmentation of plaque.

Keywords

Elastography; elasticity imaging; strain imaging; carotid plaque; motion tracking; multi-level; adventitia; vascular cognitive impairment

Introduction

Stroke is the leading cause of serious, long-term disability and the fourth leading cause of mortality in the United States (Kochanek et al. 2011). Stroke etiologies and vascular risk factors are different in young adult patients and older patients, and mortality or clinical outcome is not independently associated with age (Arnold et al. 2008). Silent strokes, without clinical symptoms, may be five times more prevalent, and are associated with cognitive impairment (Vermeer et al. 2003; Elias et al. 2004). Studies have shown that the risk of silent stroke is positively related to the extent of carotid stenosis for both symptomatic and asymptomatic patients (Norris and Zhu 1992). Silent stroke and cognition decline may occur with concurrent subclinical emboli (Dempsey et al. 2010), which can flow into the vasculature of brain and lead to ischemic events resulting in stroke, vascular cognitive impairment or both (Whisnant et al. 1990).

To assess cognitive impairment, the Repeatable Battery for the Assessment of Neuropsychological Status (RBANS) (Randolph et al. 1998) has been widely used as a cognition test protocol. The RBANS takes less than 30 minutes to administer, evaluating five cognitive domains. This test battery is effective at both characterizing cognitive decline in older patients and screening for dementia in younger patients (Randolph et al. 1998). In addition, age- and education-corrected norms have been provided (Duff et al. 2003). More recently, the National Institute of Neurological Disorder and Stroke-Canadian Stroke Network (NINDS-CSN) has published the Vascular Cognitive Impairment Harmonization Standards (Hachinski et al. 2006). Like the RBANS, the 60-minute battery recommended by the NINDS-CSN captures several functional domains. These testing standards have been used to assess vascular cognitive impairment (Gorelick et al. 2011), and have been incorporated into standardized stroke patient care with demonstrated clinical feasibility (Han et al. 2014).

Cognitive impairment may be related to cerebral micro-emboli (Russell 2002). Emboli might be generated from rupture of vulnerable plaques--- a thin fibrous cap or fissured cap covering the foamy or necrotic core, with the presence of overt hemorrhage, ulceration or thrombus (Stary 1992; Stary et al. 1995)--- thus it is clinically important to assess plaque vulnerability (Carr et al. 1996). Ultrasound elastography has been gaining more recognition

in plaque characterization, since increased deformation and strain in the plaque has been associated with cognition decline through embolization (Rocque et al. 2012; Wang et al. 2014) (Varghese 2009). Majdouline et al. (2014) investigated the condition of the plaque and associated shear strain elasticity index (SSE), with its absolute value statistically higher in plaques with increased vulnerability (Majdouline et al. 2014). Mercure et al. (2014) corrected the under-estimation of axial strain in plaques using a kinematics constraint-based local angle compensation method (Mercure et al. 2014). Naim et al. (2013) found that strain index can index the presence of a lipid core with high sensitivity and moderate specificity, using clinical findings from high resolution magnetic resonance imaging (MRI) (Naim et al. 2013). Liu et al. (2015) recently utilized a two-level, RF data based real-time tissue elastography (RTE) to identify vulnerable carotid atherosclerotic plaques (Liu et al. 2015). They showed that ultrasonic RTE has the potential to characterize composition of carotid plaques *in vivo* and identify plaques that are vulnerable to rupture. Ramnarine et al. (2014) recently conducted a study involving eighty-one patients and demonstrated that shear wave elastography (SWE) is able to quantify carotid plaque elasticity and provide clinically relevant information to help identify unstable carotid plaques (Ramnarine et al. 2014). Widman et al. (2015) compared shear moduli of hard and soft plaques in vessel phantoms measured using SWE to mechanical testing results, and validated the feasibility of characterizing *in vivo* carotid plaque using SWE (Widman et al. 2015). Korukonda et al. (2013) studied sparse-array elastography and compared it to plane-wave imaging and compounded-plane-wave imaging on simulated vessel and vessel phantoms (Korukonda et al. 2013). They concluded that the performance of sparse-array imaging was comparable to plane-wave and compounded-plane-wave imaging on phantoms. Hansen et al. (2014) recently extended their strain compounding technique to plane-wave based ultrafast ultrasonic imaging (Hansen et al. 2014).

In our laboratory, a robust strain estimation algorithm utilizing a hierarchical framework was developed to estimate accumulated strain indices over a cardiac cycle in carotid plaque (McCormick et al. 2012). Accumulated axial and lateral strain indices were shown to be capable of assessing vulnerability of carotid plaque in human subjects, and were significantly correlated with cognitive impairment (Shi et al. 2008; Wang et al. 2014), and increases in white matter hyperintensities (WMH) (Berman et al. 2015), (bright regions on T2 weighted brain MRI due to cumulative subclinical microvascular injury). We have also recently illustrated that shear strain indices obtained with the inclusion of the adventitial layer demonstrated significant correlations with cognitive function in human subjects (Wang et al. 2015). In this paper, we combine a newer group of patients with the earlier group that we had reported before to obtain a larger sample size and therefore increase statistical power, and evaluate the correlation between strain indices and cognitive function, as well as the feasibility of using strain indices to classify cognitive impairment.

Materials and Methods

Data acquisition

Ultrasound imaging and cognition tests were performed on 75 patients (44 male and 31 female) who presented with significant plaque prior to carotid endarterectomy (CEA)

procedure at the University of Wisconsin-Madison Hospitals and Clinics. All enrolled patients met surgical guidelines for CEA with > 60% stenosis of the carotid artery based on the North American Symptomatic Carotid Endarterectomy Trial (NASCET) and Asymptomatic Carotid Artery Stenosis (ACAS) criteria (NASCET 1991; ACAS 1995). Symptomatic patients presented with classical stroke symptoms such as motor and/or language deficits or transient ischemic attacks (TIA). Asymptomatic patients on the other hand did not present with classical stroke deficits, but may have had silent strokes seen on diagnostic imaging. Patients participated in the study after providing informed consent using a protocol approved by the University of Wisconsin-Madison Institutional Review Boards (IRB). The age of the patients ranged from 43 to 85, with a mean and standard deviation of 68.65 ± 9.23. The first group of 24 patients participated in the study before 2011, and a second group of 51 patients participated since 2011.

Ultrasound radiofrequency (RF) echo signal data was acquired, along with clinical B-mode images and color-flow Doppler images on these patients. A Siemens Antares ultrasound system (Siemens Ultrasound, Mountain View, CA, USA) equipped with a VFX 13-5 linear array transducer was used to acquire ultrasound data on the first group of 24 patients, while a Siemens S2000 ultrasound system (Siemens Ultrasound, Mountain View, CA, USA) equipped with a 18L6 linear array transducer was used on the second group of 51 patients. Although different transducers and different ultrasound systems were utilized, the transmit frequency was set to 11.4 MHz for both transducers and on both systems. The sampling frequency of 40 MHz was also the same for both ultrasound systems with a single transmit focus set at the depth of the plaque. The RF echo signal properties and the signal processing utilized were similar for both the data sets acquired.

Strain indices estimation

We used the same strain estimation algorithm on all patients regardless of the ultrasound system. Plaque regions with adventitia were segmented by a radiologist/research sonographer for end-diastole frames using the Medical Imaging Interaction Toolkit (MITK), as shown in Figure 1. Segmentations were done on B-mode images reconstructed from RF data. Clinical B-mode images and color-flow Doppler images were also used to help determine plaque borders. RF images are viewed using MITK software over the entire cardiac cycle along with a simultaneous review of Digital Imaging and Communications in Medicine (DICOM) clinical B-mode and color-flow Doppler images, so that a side by side comparison of vessel walls and plaque borders can be made. DICOM images are stored as cine loops and still frames enabling the radiologist/research sonographer to scroll through the frames to determine plaque and vessel wall borders. The segmented regions were automatically tracked over two complete cardiac cycles using a hierarchical block-matching motion tracking algorithm developed in our laboratory (McCormick et al. 2012), using the segmented end-diastolic frame as the initial frame of the sequence. For optimal motion tracking purpose, a dynamic frame skip method was utilized with a short frame skip during systole and a long frame skip during end-diastole (McCormick et al. 2012).

Displacements between consecutive frames were tracked utilizing normalized cross-correlation analysis with recursive Bayesian regularization over three iterations (McCormick

et al. 2011), and filtered with a 3 × 3 pixel (0.06 mm × 0.225 mm) median filter. Accumulated displacements over a cardiac cycle were then utilized to estimate strain by applying a modified least squares fit over a 7 pixel length. The matching block utilized for processing was 15 × 28 pixels at the top level, and 10 × 18 pixels at the bottom level of the multi-level algorithm (McCormick et al. 2012). With no overlap between blocks, the final strain pixel resolution was 0.2 mm (axial) by 1.35 mm (lateral). For the RF data acquired, along the axial direction, one pixel represents 0.02 mm, while along the lateral direction one pixel represents 0.075 mm (McCormick et al. 2012).

Strain images computed inside the segmented region were overlaid on the corresponding B-mode images, as shown in Figure 2. Maximum accumulated strain over two cardiac cycles was then located in the strain image and averaged by the nearby 10–20 data points to reduce noise artifacts. The absolute value of the maximum strain over a cardiac cycle was used in our analysis. Although we do anticipate slightly improved strain imaging performance (in terms of the elastographic signal to noise ratio (SNRe) (Varghese and Ophir 1997)) with the Siemens S2000 and the 18L6 linear array transducer, however, this is not overtly significant after the strain accumulation over cardiac cycles used to obtain the maximum strain indices.

Cognitive assessment

Cognitive assessment was also performed before CEA. Different cognition test protocols were conducted for the two groups of patients. The first group of 24 patients were assessed using Repeatable Battery for the Assessment of Neuropsychological Status (RBANS), which provides a total score for overall cognition status, as well as five sub-scores for specific cognitive abilities including immediate memory, visuospatial/constructional, language, attention and delayed memory (Randolph et al. 1998). The second group of 51 patients were assessed using the more recent National Institute of Neurological Disorders and Stroke-Canadian Stroke Network (NINDS-CSN) Vascular Cognitive Impairment Harmonization Standards 60-minute protocol, which consists of several scores evaluating executive function/activation, visuospatial ability, language/lexical retrieval, memory/learning, neuropsychiatric/depression symptoms, and pre-morbid intelligence (Hachinski et al. 2006).

To allow data from these batteries to be combined, a z-score (Rosner 2010) representative of overall cognitive function was generated for each participant. For the first group of 24 patients, the z-scores represented the standardized score for RBANS Total (overall) performance. For the second group of 51 patients, z-scores was calculated for each sub-test of the NINDS-CNS battery, and then averaged across all sub-tests. One overall cognition z-score was thus created for each participant in both groups, allowing standardized performance to be assessed regardless of test battery.

Statistics and ROC

Ultrasound imaging and cognition assessment were conducted separately and were blinded to each other. Maximum strain indices were correlated to the standardized z-score using a Pearson's correlation coefficient r and a significance level of $p<0.05$ using a two-tailed t-test. Correlation analyses were performed in each group of patients separately, and also in all patients combined. Patients were also divided into symptomatic and asymptomatic

groups based on clinical criteria. Among the 75 patients, 47 patients were symptomatic, 27 patients were asymptomatic and one patient was questionable (cardiac symptoms) based on clinical findings.

Receiver operating characteristic (ROC) analysis was performed to evaluate the efficacy of high strain indices to predict cognitive impairment. Patients were divided into 2 groups using $z = 0$ as a threshold; a lower cognition group that was below average in total cognition scores, suggesting mild to moderate cognitive impairment, and a higher cognition group with z-score ≥ 0. The lower cognition group was assigned to the positive category, and the higher cognition group assigned to the negative category. Maximum axial, lateral and shear strain indices were used as predictors, as well as a combination of two of them, and a combination of all three indices. Using a 10-fold cross-validation logistic regression as classifier, ROC analysis for the single features and combined features were performed using Weka 3 (Version 3.7.12, Machine Learning Group at the University of Waikato) (Hall et al. 2009). Sensitivity and specificity for both single features and combined features were also computed. ROC curves were fitted using parameters (Brown and Davis 2006) generated with ROC-kit software (Version 0.9.1 beta, Metz ROC Software at the University of Chicago). The area under curve (AUC) and the upper and lower bounds of a 95% confidence interval (CI) were also estimated using ROC-kit.

Results

Correlation analyses

Figure 2 shows typical axial, lateral and shear strain images overlaid on B-mode images for the plaque segmented in Figure 1. The magnitude and direction of strains are also depicted on the color bar. Positive strain represents expansion of the vessel wall and plaque, while negative strains represent compression. The distribution and variation of strain inside the plaque indicates plaque heterogeneity. Note that the composition or tissue type of plaque changes from region to region within a single plaque. Higher strains are observed at the vessel wall - plaque interface close to adventitia, especially for shearing strains.

Figure 3 presents plots of correlations of cognitive z-scores with maximum axial, lateral and shear strain indices for all patients, and for symptomatic and asymptomatic groups separately. A linear fit was performed for all patients, and also for the two groups respectively. Correlation coefficients and significance values for all analyses are shown in Table 1. Correlations utilizing the RBANS Total score for the first group of 24 patients have been reported previously (Wang et al. 2015). Briefly, we found that cognitive ability decreased with increasing strain indices, indicating that higher strain indices are associated with lower cognitive function. The correlation coefficient was smaller when the two groups of patients (i.e., those completing the RBANS versus NINDS-CNS battery) were combined, while remaining significant at $p < 0.05$.

ROC analysis

Figure 4 presents a three-dimensional scatter plot of the maximum axial, lateral and shear strain indices against each other for the lower cognition group ($z < 0$) and the higher

cognition group ($z \geq 0$). The strain indices are presented in a log scale to clearly visualize variations in the indices between individual patients. Although some overlap exist between the two groups, it can be seen that the lower cognition group tends to have higher strain indices, while the higher cognition group tends to cluster in the region with lower strain indices range, suggesting the possibility of using maximum strain indices to differentiate between the lower cognition group and the higher cognition groups, respectively.

Figures 5 depicts the comparisons of ROC curves for the maximum axial, lateral and shear strain indices individually and in combination to predict cognition decline for all patients. The sensitivity, specificity, AUC and 95% CI for each classifier are listed in Table 2. The AUC values for the seven individual and group of indices lie between 0.75 and 0.8, suggesting a good detection performance. Lateral strain indices exhibit the best performance with an AUC of 0.79. However, there was no significant improvement with the combination of strain indices, indicating that the strain indices are not completely independent of each other.

Similar ROC analyses were also conducted for the symptomatic patients only and for the asymptomatic patients only. The ROC curves for symptomatic group and for asymptomatic group are illustrated in Figure 6 and Figure 7, respectively. The sensitivity, specificity, AUC and 95% CI for symptomatic group and for asymptomatic group are listed in Table 3 and Table 4, respectively. For the symptomatic group, the AUC values improve to be between 0.78 and 0.85. Lateral strain individually, and the combination of lateral and shear strain provide the best performance with an AUC of 0.85. For the asymptomatic group, the AUC values are not as high, between 0.59 and 0.69. Among all classifiers, lateral strain indices provide the best performance with an AUC of 0.68. The comparison between different groups of patients indicates that the performance of maximum strain indices to predict cognitive impairment is better for symptomatic patients. Similarly, there was no significant improvement with the combination of features, for both symptomatic and asymptomatic patient groups as observed for the entire group of patients.

Discussion

In this paper, we have shown that the evaluation of cognition using standardized total function scores shows significant correlations with the maximum strain indices. The primary reason for combining the two groups of patients was to obtain a larger sample size and thereby a more robust prediction model. The negative association indicates that patients with higher strain indices tend to perform poorly on cognitive assessment relative to other participants. This relationship was also supported by what was observed in the three-dimensional scatter plot for the lower cognition group and the higher cognition group, respectively. This is consistent with our hypothesis that micro-emboli that may lead to cognitive impairment, possibly resulting from the rupture of vulnerable plaque that manifest with increased strain, since higher strain suggests larger deformation and increased probability of plaque rupture. Despite the statistically significant correlation described in this paper, examination of a larger number of patients is essential to further understand this relationship.

Note that correlation of cognitive function with the maximum lateral strain indices is much higher for symptomatic patients than asymptomatic patients. This is consistent with our hypothesis that plaque in symptomatic patients may have ruptured previously, resulting in increased lateral strain with possible fissures compared to the possibly intact plaque in asymptomatic patients. For asymptomatic patients, the plaque might still be intact, thus the fibrous cap may limit the deformation of plaque in the lateral direction. However, softer plaque regions with increased strain or deformation in asymptomatic plaque may eventually break off and generate emboli.

Overall, we demonstrated the feasibility of classifying and determining patients at higher risk of cognitive impairment using maximum strain indices. The improved performance of high strain indices to indirectly predict cognitive impairment in symptomatic patients than that in asymptomatic patients is as expected, since asymptomatic patients by definition are those who are devoid of possible clinical symptoms, suggesting there might be other pathways to cognitive decline, in addition to embolization. Comparison of ROC curves for symptomatic patients and asymptomatic patients reveal that the etiology of cognitive decline might be different for symptomatic patients and asymptomatic patients. Carotid plaque instability might be an important etiology of vascular cognitive decline for symptomatic patients.

We have shown previously that it is essential to include adventitia into plaque segmentation, since higher shearing strain might occur at the interface of plaque and vessel wall (Wang et al. 2015). In this paper we also observed higher strains at the border of plaque and at the vessel wall - plaque interface, especially in the shear strain images. The fact that all correlations are significant when we include adventitia in the strain analysis further proves the feasibility of the plaque-with-adventitia segmentation method, and supports theories of the importance of the vessel wall - plaque interface in the pathophysiology of embolic disease. Our future work will include investigations on whether plaque strain indices correlate to plaque echogenicity (Kanber et al. 2015), and other ultrasound B-mode image features.

Conclusions

In summary, we demonstrated significant correlations between maximum strain indices and overall cognitive function, and the feasibility of using these maximum strain indices to predict cognitive decline. Although, we cannot conclusively state that the cognitive decline in the patients studied was only due to micro-emboli. The significant correlation ($p < 0.05$) and AUC values visualized in the ROC curves suggest that strain indices obtained in the plaque with the inclusion of adventitia may assist in the characterization of vulnerable plaque and identification of plaque prone to rupture. Ultrasound strain imaging can therefore play an important role in the prediction of embolism from vulnerable plaque and resulting cognitive impairment. Predication based on AUC values are better for symptomatic when compared to asymptomatic patients. Strain indices may in the future be utilized to differentiate between patients requiring surgical intervention versus more conservative medical therapies.

Acknowledgments

This work was supported in part by NIH grants R21 EB010098-02, R01 NS064034-05, and 2R01 CA112192-07. This research was performed using the computational resources provided by the UW-Madison Center For High Throughput Computing (CHTC) in the Department of Computer Sciences. The CHTC is supported by UW-Madison and the Wisconsin Alumni Research Foundation, and is an active member of the Open Science Grid, which is supported by the National Science Foundation and the U.S. Department of Energy's Office of Science. The authors would like to thank Ms. Pamela Winne for coordinating the data acquisition on patients.

References

ACAS. Endarterectomy for asymptomatic carotid artery stenosis. Executive Committee for the Asymptomatic Carotid Atherosclerosis Study. JAMA. 1995; 273:1421–1428. [PubMed: 7723155]

Arnold M, Halpern M, Meier N, Fischer U, Haefeli T, Kappeler L, Brekenfeld C, Mattle HP, Nedeltchev K. Age-dependent differences in demographics, risk factors, co-morbidity, etiology, management, and clinical outcome of acute ischemic stroke. J Neurol. 2008; 255:1503–1507. [PubMed: 18677634]

Berman S, Wang X, Mitchell CC, Kundu B, Jackson DC, Wilbrand SM, Varghese T, Hermann BP, Rowley H, Johnson SC, Dempsey RJ. The relationship between carotid artery plaque stability and white matter ischemic injury. NeuroImage: Clinical. 2015; 9:216–222. [PubMed: 26448914]

Brown CD, Davis HT. Receiver operating characteristics curves and related decision measures: A tutorial. Chemometr Intell Lab. 2006; 80:24–38.

Carr S, Farb A, Pearce WH, Virmani R, Yao JS. Atherosclerotic plaque rupture in symptomatic carotid artery stenosis. J Vasc Surg. 1996; 23:755–765. discussion 65-6. [PubMed: 8667496]

Dempsey RJ, Vemuganti R, Varghese T, Hermann BP. A review of carotid atherosclerosis and vascular cognitive decline: a new understanding of the keys to symptomology. Neurosurgery. 2010; 67:484–493. discussion 93-4. [PubMed: 20644437]

Duff K, Patton D, Schoenberg MR, Mold J, Scott JG, Adams RL. Age- and education-corrected independent normative data for the RBANS in a community dwelling elderly sample. Clin Neuropsychol. 2003; 17:351–366. [PubMed: 14704885]

Elias MF, Sullivan LM, D'Agostino RB, Elias PK, Beiser A, Au R, Seshadri S, DeCarli C, Wolf PA. Framingham stroke risk profile and lowered cognitive performance. Stroke. 2004; 35:404–409. [PubMed: 14726556]

Gorelick PB, Scuteri A, Black SE, Decarli C, Greenberg SM, Iadecola C, Launer LJ, Laurent S, Lopez OL, Nyenhuis D, Petersen RC, Schneider JA, Tzourio C, Arnett DK, Bennett DA, Chui HC, Higashida RT, Lindquist R, Nilsson PM, Roman GC, Sellke FW, Seshadri S. Vascular contributions to cognitive impairment and dementia: a statement for healthcare professionals from the american heart association/american stroke association. Stroke. 2011; 42:2672–2713. [PubMed: 21778438]

Hachinski V, Iadecola C, Petersen RC, Breteler MM, Nyenhuis DL, Black SE, Powers WJ, DeCarli C, Merino JG, Kalaria RN, Vinters HV, Holtzman DM, Rosenberg GA, Wallin A, Dichgans M, Marler JR, Leblanc GG. National Institute of Neurological Disorders and Stroke-Canadian Stroke Network vascular cognitive impairment harmonization standards. Stroke. 2006; 37:2220–2241. [PubMed: 16917086]

Hall M, Frank E, Holmes G, Pfahringer B, Reutemann P, Witten IH. The WEKA data mining software: an update. ACM SIGKDD explorations newsletter. 2009; 11:10–18.

Han DY, Anderson AJ, Jones JE, Hermann BP, Sattin JA. Neuropsychology in Multidisciplinary Stroke Care: Clinical Feasibility of the NINDS-CSN Vascular Cognitive Impairment Harmonization Standards. International Scholarly Research Notices. 2014; 2014:6.

Hansen HHG, Saris AECM, Vaka NR, Nillesen MM, de Korte CL. Ultrafast vascular strain compounding using plane wave transmission. J Biomech. 2014; 47:815–823. [PubMed: 24484646]

Kanber B, Hartshorne TC, Horsfield MA, Naylor AR, Robinson TG, Ramnarine KV. A Novel Ultrasound-Based Carotid Plaque Risk Index Associated with the Presence of Cerebrovascular Symptoms. Ultraschall Med. 2015; 36:480–486. [PubMed: 25389913]

Kochanek KD, Xu J, Murphy SL, Minino AM, Kung HC. Deaths: final data for 2009. Natl Vital Stat Rep. 2011; 60:1–116. [PubMed: 24974587]

Korukonda S, Nayak R, Carson N, Schifitto G, Dogra V, Doyley MM. Noninvasive vascular elastography using plane-wave and sparse-array imaging. IEEE Trans Ultrason Ferroelectr Freq Control. 2013; 60:332–342. [PubMed: 23357907]

Liu F, Yong Q, Zhang Q, Liu P, Yang Y. Real-time tissue elastography for the detection of vulnerable carotid plaques in patients undergoing endarterectomy: a pilot study. Ultrasound Med Biol. 2015; 41:705–712. [PubMed: 25619789]

Majdouline Y, Ohayon J, Keshavarz-Motamed Z, Roy Cardinal MH, Garcia D, Allard L, Lerouge S, Arsenault F, Soulez G, Cloutier G. Endovascular shear strain elastography for the detection and characterization of the severity of atherosclerotic plaques: in vitro validation and in vivo evaluation. Ultrasound Med Biol. 2014; 40:890–903. [PubMed: 24495438]

McCormick M, Rubert N, Varghese T. Bayesian regularization applied to ultrasound strain imaging. IEEE Trans Biomed Eng. 2011; 58:1612–1620. [PubMed: 21245002]

McCormick M, Varghese T, Wang X, Mitchell C, Kliewer MA, Dempsey RJ. Methods for robust in vivo strain estimation in the carotid artery. Phys Med Biol. 2012; 57:7329–7353. [PubMed: 23079725]

Mercure E, Destrempes F, Roy Cardinal MH, Poree J, Soulez G, Ohayon J, Cloutier G. A local angle compensation method based on kinematics constraints for non-invasive vascular axial strain computations on human carotid arteries. Comput Med Imaging Graph. 2014; 38:123–136. [PubMed: 24050884]

Naim C, Cloutier G, Mercure E, Destrempes F, Qin Z, El-Abyad W, Lanthier S, Giroux MF, Soulez G. Characterisation of carotid plaques with ultrasound elastography: feasibility and correlation with high-resolution magnetic resonance imaging. Eur Radiol. 2013; 23:2030–2041. [PubMed: 23417249]

NASCET. North American Symptomatic Carotid Endarterectomy Trial. Methods, patient characteristics, and progress. Stroke. 1991; 22:711–720. [PubMed: 2057968]

Norris JW, Zhu CZ. Silent stroke and carotid stenosis. Stroke. 1992; 23:483–485. [PubMed: 1561676]

Ramnarine KV, Garrard JW, Kanber B, Nduwayo S, Hartshorne TC, Robinson TG. Shear wave elastography imaging of carotid plaques: feasible, reproducible and of clinical potential. Cardiovasc Ultrasound. 2014; 12:49. [PubMed: 25487290]

Randolph C, Tierney MC, Mohr E, Chase TN. The Repeatable Battery for the Assessment of Neuropsychological Status (RBANS): preliminary clinical validity. J Clin Exp Neuropsychol. 1998; 20:310–319. [PubMed: 9845158]

Rocque BG, Jackson D, Varghese T, Hermann B, McCormick M, Kliewer M, Mitchell C, Dempsey RJ. Impaired cognitive function in patients with atherosclerotic carotid stenosis and correlation with ultrasound strain measurements. J Neurol Sci. 2012; 322:20–24. [PubMed: 22658531]

Rosner B. Fundamentals of biostatistics. Cengage Learning. 2010

Russell D. Cerebral microemboli and cognitive impairment. J Neurol Sci. 2002; 203:204–211.

Shi H, Mitchell CC, McCormick M, Kliewer MA, Dempsey RJ, Varghese T. Preliminary in vivo atherosclerotic carotid plaque characterization using the accumulated axial strain and relative lateral shift strain indices. Phys Med Biol. 2008; 53:6377–6394. [PubMed: 18941278]

Stary HC. Composition and classification of human atherosclerotic lesions. Virchows Arch A Pathol Anat Histopathol. 1992; 421:277–290. [PubMed: 1413492]

Stary HC, Chandler AB, Dinsmore RE, Fuster V, Glagov S, Insull W Jr, Rosenfeld ME, Schwartz CJ, Wagner WD, Wissler RW. A definition of advanced types of atherosclerotic lesions and a histological classification of atherosclerosis. A report from the Committee on Vascular Lesions of the Council on Arteriosclerosis, American Heart Association. Circulation. 1995; 92:1355–1374. [PubMed: 7648691]

Varghese T. Quasi-Static Ultrasound Elastography. Ultrasound Clin. 2009; 4:323–338. [PubMed: 20798841]

Varghese T, Ophir J. A theoretical framework for performance characterization of elastography: the strain filter. IEEE Trans Ultrason Ferroelectr Freq Control. 1997; 44:164–172. [PubMed: 18244114]

Vermeer SE, Prins ND, den Heijer T, Hofman A, Koudstaal PJ, Breteler MM. Silent brain infarcts and the risk of dementia and cognitive decline. N Engl J Med. 2003; 348:1215–1222. [PubMed: 12660385]

Wang X, Jackson DC, Varghese T, Mitchell CC, Hermann BP, Kliewer MA, Dempsey RJ. Correlation of cognitive function with ultrasound strain indices in carotid plaque. Ultrasound Med Biol. 2014; 40:78–89. [PubMed: 24120415]

Wang X, Mitchell C, Varghese T, Jackson D, Rocque B, Hermann B, Dempsey R. Improved Correlation of Strain Indices with Cognitive Dysfunction with Inclusion of Adventitial Layer with Carotid Plaque. Ultrasonic Imaging. 2015 0161734615589252.

Whisnant JP, Basford JR, Bernstein EF, Cooper ES, Dyken ML, Easton JD, Little JR, Marler JR, Millikan CH, Petito CK, Price TR, Raichle ME, Robertson JT, Thiele B, Walker MD, Zimmerman aRA. Special report from the National Institute of Neurological Disorders and Stroke. Classification of cerebrovascular diseases III. Stroke. 1990; 21:637–676. [PubMed: 2326846]

Widman E, Maksuti E, Larsson D, Urban MW, Bjallmark A, Larsson M. Shear wave elastography plaque characterization with mechanical testing validation: a phantom study. Phys Med Biol. 2015; 60:3151–3174. [PubMed: 25803520]

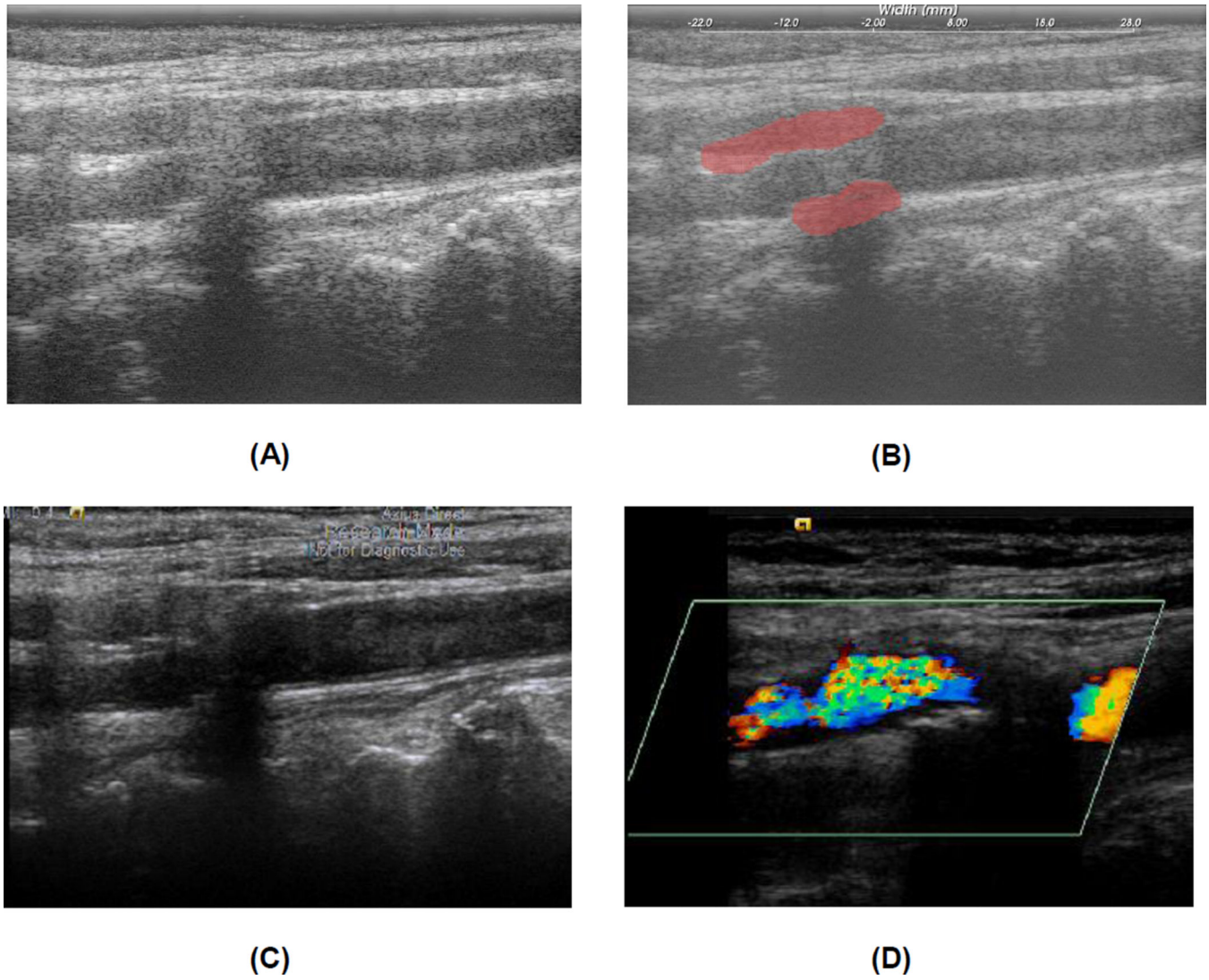

Figure 1.

B-mode image reconstructed from RF data (A) and segmented plaque with adventitia on the B-mode image (B). Clinical DICOM Image with the 18L6 Transducer in same plane as RF acquisition (C). Cropped color flow Doppler DICOM image demonstrating color flow in the lumen assisting with plaque border definition (D).

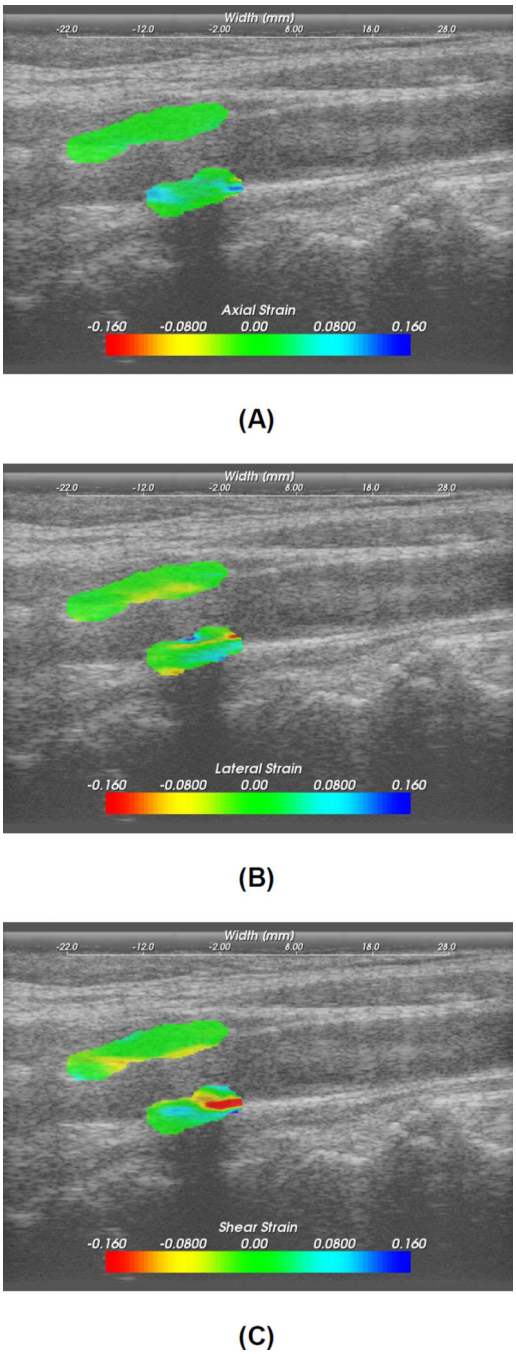

Figure 2.
Axial (A), lateral (B) and shear (C) strain images in the segmented region overlaid on the B-mode image.

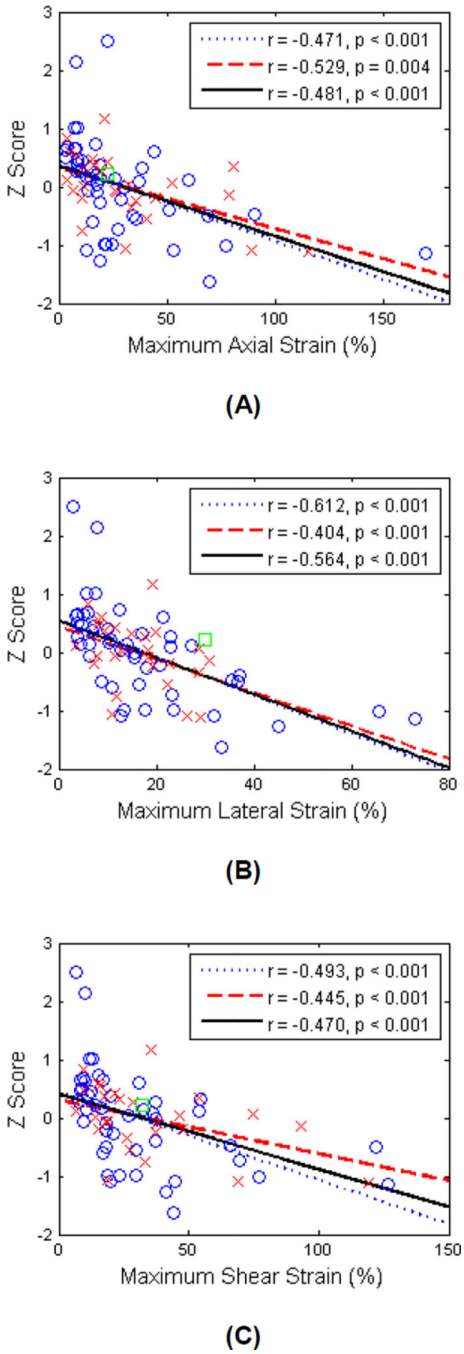

Figure 3.

Linear least-squares fits of the z-scores with maximum axial strain (A), maximum lateral strain (B) and maximum shear strain (C). ○ = Symptomatic, × = asymptomatic, □ = questionable, the dotted line represents the linear fit for symptomatic, dashed line the linear fit for asymptomatic, and the solid line denotes the linear fit for all patients.

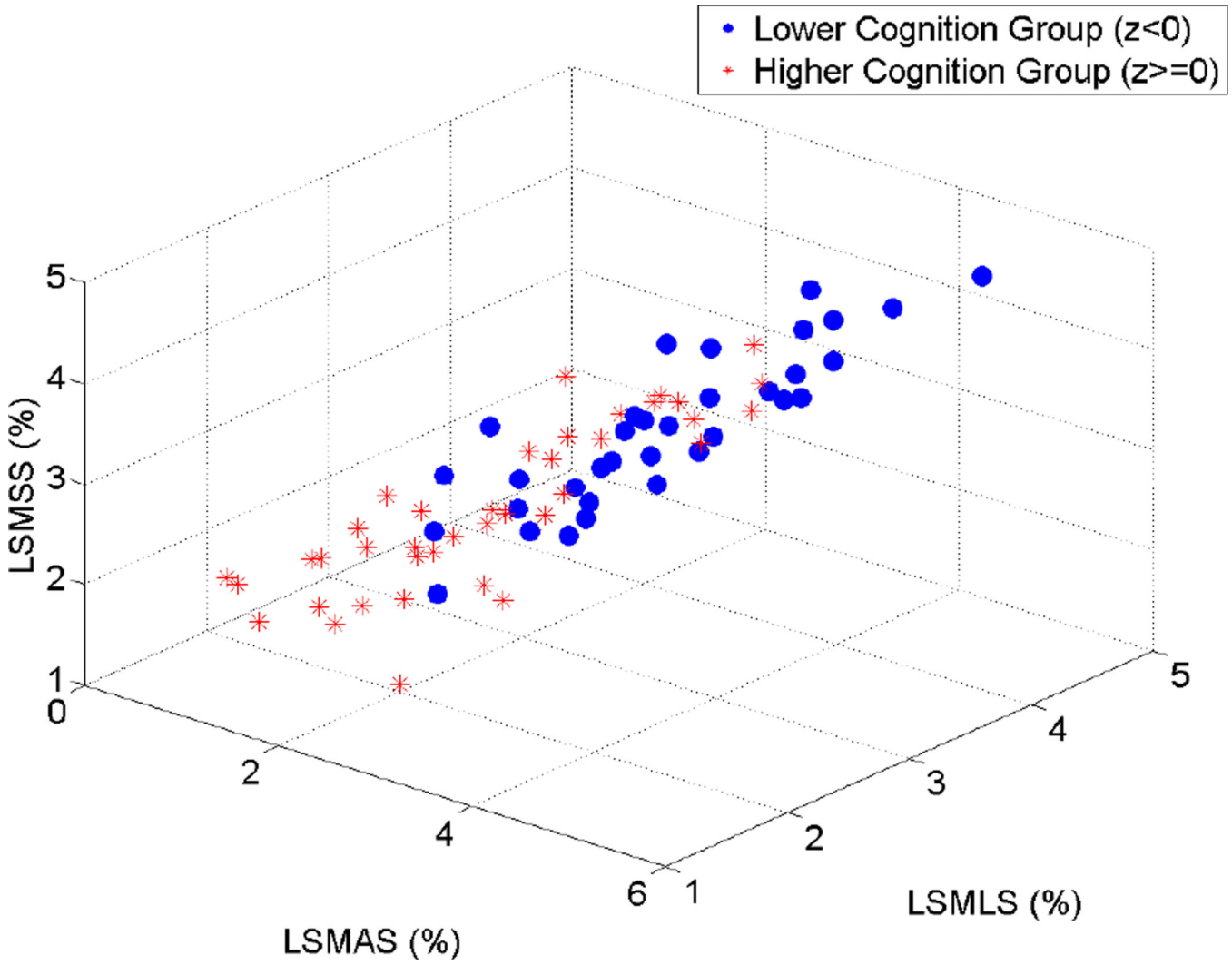

Figure 4.

Three-dimensional scatter plot of maximum axial, lateral and shear strain indices plotted against each other. ○ = Lower cognition group (z<0), * = higher cognition group (z≥0). LSMAS = Log-scaled maximum axial strain, LSMLS = log-scaled maximum lateral strain, LSMSS = log-scaled maximum shear strain.

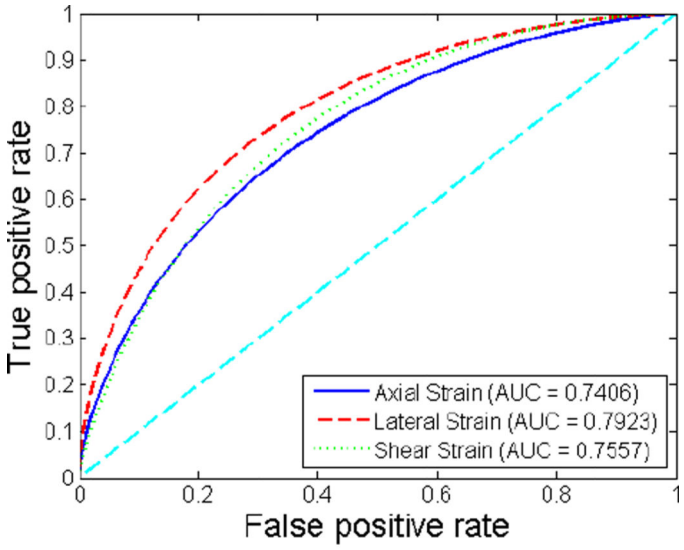

(A)

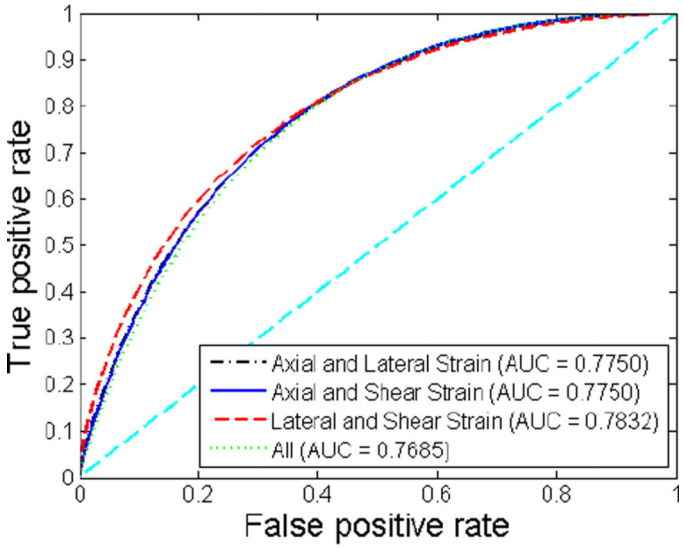

(B)

Figure 5.
ROC curves using individual strain indices or features (A) and combined features (B) for all patients. The diagonal reference line is also shown in the plots.

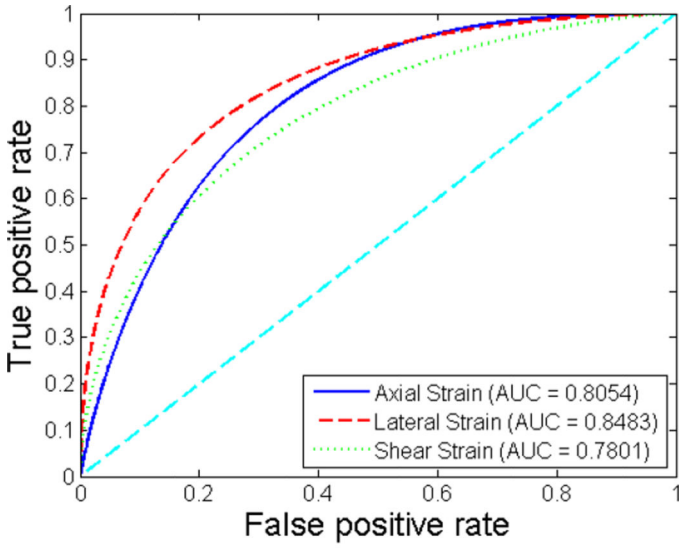

(A)

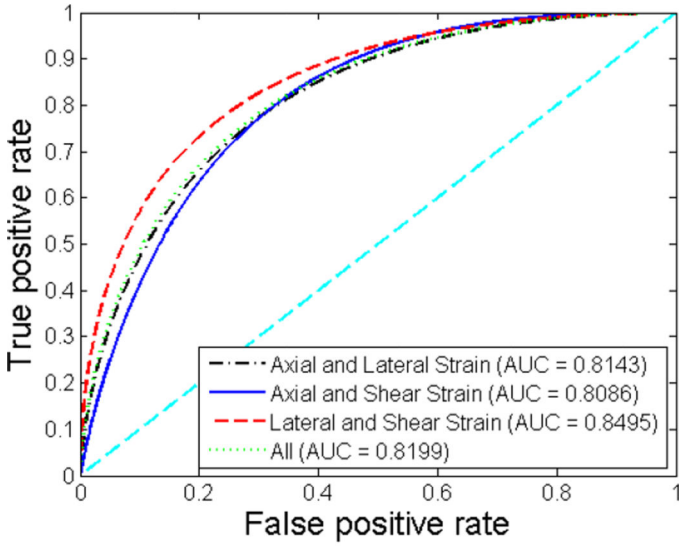

(B)

Figure 6.

ROC curves using individual features (A) and combined features (B) for symptomatic patients. The diagonal reference line is also shown in the plots.

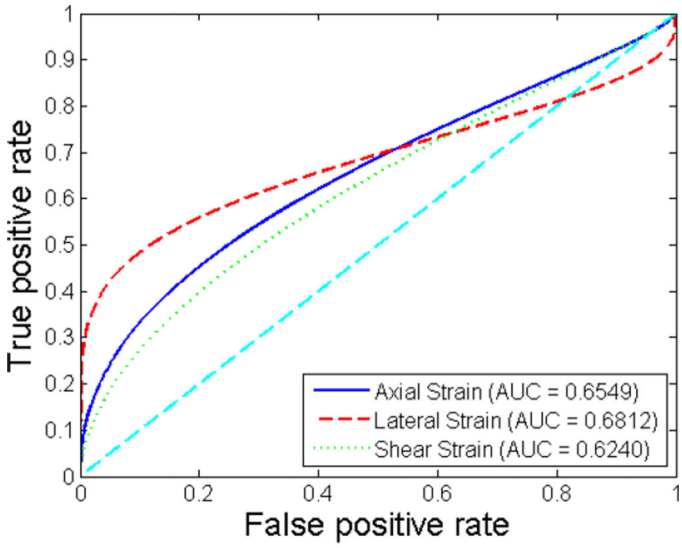

(A)

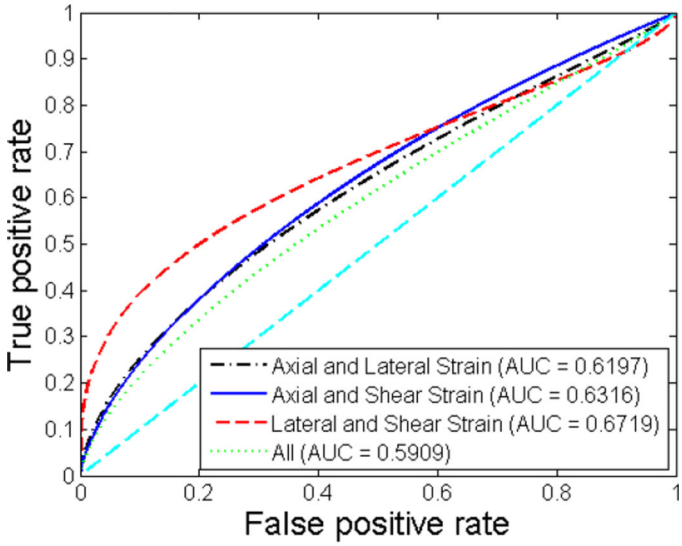

(B)

Figure 7.

ROC curves using individual features (A) and combined features (B) for asymptomatic patients. The diagonal reference line is also shown in the plots.

Table 1

Correlation of z-score to maximum strain indices.

	Axial Strain	Lateral Strain	Shear Strain
All (n=75)	$r = -0.481$, $p < 0.001$	$r = -0.564$, $p < 0.001$	$r = -0.470$, $p < 0.001$
First group (n = 24)	$r = -0.581$, $p = 0.003$	$r = -0.656$, $p < 0.001$	$r = -0.717$, $p < 0.001$
Second group (n = 51)	$r = -0.597$, $p < 0.001$	$r = -0.592$, $p < 0.001$	$r = -0.590$, $p < 0.001$
Symptomatic (n=47)	$r = -0.471$, $p < 0.001$	$r = -0.612$, $p < 0.001$	$r = -0.493$, $p < 0.001$
Asymptomatic (n=27)	$r = -0.529$, $p = 0.004$	$r = -0.404$, $p < 0.001$	$r = -0.445$, $p < 0.001$

Table 2

Sensitivity, specificity, area under curve (AUC) and 95% confidence intervals (CI) for individual features and combined features for all patients.

	Sensitivity	**Specificity**	**AUC**	**95% (CI_{upper}−CI_{lower})**
Axial Strain	0.667	0.633	0.7406	0.8382−0.6191
Lateral Strain	0.693	0.675	0.7923	0.8781−0.6785
Shear Strain	0.653	0.622	0.7557	0.8503−0.6358
Axial and Lateral Strain	0.653	0.632	0.7750	0.8647−0.6587
Axial and Shear Strain	0.640	0.601	0.7750	0.8648−0.6587
Lateral and Shear Strain	0.707	0.686	0.7832	0.8710−0.6683
All	0.680	0.649	0.7685	0.8600−0.6507

Table 3

Sensitivity, specificity, area under curve (AUC) and 95% confidence intervals (CI) for individual features and combined features for symptomatic patients.

	Sensitivity	**Specificity**	**AUC**	**95% (CI_{upper}–CI_{lower})**
Axial Strain	0.681	0.641	0.8054	0.9051–0.6596
Lateral Strain	0.723	0.703	0.8483	0.9326–0.7133
Shear Strain	0.638	0.607	0.7801	0.8892–0.6267
Axial and Lateral Strain	0.723	0.703	0.8143	0.9105–0.6714
Axial and Shear Strain	0.681	0.641	0.8086	0.9069–0.6640
Lateral and Shear Strain	0.723	0.694	0.8495	0.9333–0.7147
All	0.723	0.694	0.8199	0.9143–0.6781

Table 4

Sensitivity, specificity, area under curve (AUC) and 95% confidence intervals (CI) for individual features and combined features for asymptomatic patients.

	Sensitivity	**Specificity**	**AUC**	**95% (CI_{upper}−CI_{lower})**
Axial Strain	0.667	0.652	0.6549	0.8330−0.4329
Lateral Strain	0.630	0.629	0.6812	0.8582−0.4483
Shear Strain	0.593	0.583	0.6240	0.8115−0.4007
Axial and Lateral Strain	0.667	0.663	0.6197	0.8058−0.4000
Axial and Shear Strain	0.667	0.652	0.6316	0.8141−0.4125
Lateral and Shear Strain	0.667	0.663	0.6719	0.8458−0.4490
All	0.741	0.732	0.5909	0.7834−0.3721